X-ray Convergent Beam Pattern Simulation Using the Moodie-Wagenfeld Equations: 3-Beam Laue Case

Linda Liu and P. Goodman

School of Physics, University of Melbourne, Parkville, Victoria, Australia 3052,
E-mail: pag@phyics.unimelb.edu.au

Dedicated to Prof. A.F. Moodie on the occasion of his 75th. birthday.

Abstract

Pattern simulations for 3-beam X-ray diffraction are presented, by multi-slice calculations based on Moodie and Wagenfeld's formulation of the X-ray equations, which factorise Maxwell's equations into Dirac format, using circular-polarisation bases.

The results are presented in the form of convergent-beam patterns for each diffraction order, using experience gained from CBED (convergent beam electron diffraction) and LACBED (large-angle CBED), since this displays the results in the most compact form. The acronym CBXRAD (convergent-beam X-ray-diffraction) is used for these patterns. Although optics required for the complete patterns is not currently available, capillary focussing is undergoing rapid development, and our simulations define critical angular ranges within reach of current designs.

Simulations for light and heavy-atoms structures belonging to the enantiomorphic space-group pair $P3_121$ and $P3_221$, provide clear evidence of chiral interaction between radiation and structure, highlighting divergences from the well-studied CBED pattern symmetries. $MoK\alpha_1$ and $TaK\alpha_1$ wavelengths were used to minimise absorption for the two structures respectively, although "anomalous absorption" is always important due to the large thicknesses required (up to 20 mm).

1. Introduction

Earlier, wedge-crystals have been used to study the effect of polarisation scattering in 2-beam X-ray transmission on an unpolarised incident beam (Hart and Milne, 1964), using a Lang camera (Lang, 1962), which used a moving table holding a

wedged crystal, and recording the results for one diffraction order as a function of thickness. Hart and Lang (1965) then observed the periodic fading and re-emerging of pendellösung fringe amplitude with thickness, arising from the beating of the two frequencies expected from the two independent linear polarisation states σ and π, using wedge crystals of Si and Ge. Following this, observations were made using linear polarised radiation incident at 45° to the 2-beam scattering vector (Skalicky and Malgrange, 1972), which showed that this periodic beating could be observed with a polariser in the incident beam. This observation immediately suggested that treatment of the whole scattering as two sets of coupled harmonic oscillators could greatly simplify future analyses of Laue-case fringes, an analysis in which the beating is treated by considering both momentum and polarisation states as taking part in a coupled coherent system. This layout of the problem then allows simple extension to N-beam coupling with $N > 2$, the simplest being the 3-beam case. This is the smallest interaction for which the structure phases play a part.

The direct factorisation of the whole transmission case as coupled equations for left and right circular polarisation states (Moodie and Wagenfeld, 1975) then invited consideration of these cases, with the additional interest of exploiting the behaviour of circularly polarised states.

Until quite recently however an experimental method sufficiently sensitive to detect such weak effects as the chiral interaction between beam and structure was lacking. The recent development and testing of capillary optics on a synchrotron source which showed that a capillary focus could be used to produce divergent-beam elastically-scattered diffraction orders using synchrotron radiation (Thiel, Stern, Bilderback and Lewis, 1989; Engström *et al.*, 1991; Bilderback, Thiel, Pahl and Brister, 1994; Baliac *et al.*, 1996), prompted a fresh look at the Wagenfeld and Moodie equations, to examine the order-of-magnitude of 3-dimensional X-ray-scattering interactions of structural interest. The advantage of capillary optics is that in principle, all the 3-dimensional data could be collected from a single CBXRAD pattern from a single diffraction order. This concentration of incident energy into one pattern

should help overcome the loss of energy in using both a polariser (1/4 wave plate) and analyser in the detector path.

It may have been forgotten, or never properly appreciated, that prior to the Wagenfeld-Moodie publication (Moodie and Wagenfeld, 1972), the factorisation of Maxwell's equations in that Dirac-equation form was considered viable only for vacuum-state propagation (e.g. Sakurai, 1967), although there have been some theoretical effort put into presenting Maxwell's equations in spinor form for visible light (Hillion, 1979), but the accurate solution presented applies only to a medium of constant refractive index. However with use of the multi-slice method, which treats the 3-dimensional problem as a series of projected-structure phase-gratings of zero thickness, and where all the propagation is in the vacuum state (Goodman and Moodie, 1974), it is clear this treatment is valid also in diffraction through a finite and periodically-modulated refractive medium. Given that X-ray scattering amplitudes are an order-of-magnitude weaker than their electron-scattering counterpart, for which the multi-slice method has already been thoroughly tested, the multi-slice treatment can assumed to be very accurate when fractional unit cell slices are used, even for the heaviest atom.

2. Nomenclature

It is appropriate here to outline the differences adopted in X-ray and electron-diffraction literature in their theoretical development. Since the broad principles involved in the two subjects are the same, it is largely historical developments which have lead to independent formulations and nomenclature. This section may also be timely, since the most recent review by Weckert and Hümmer (1997) of Multiple-Beam X-Ray Diffraction uses the standard eigen-value treatment for Maxwell's equations, and deals almost exclusively with the determination of absolute configuration in organic compounds whose heaviest atom is nitrogen, and for as-grown crystals of 0.1 to 0.5 mm, and they are able to distinguish between use of anomalous absorption and use of 3-beam interference as separate methods. With thick

heavy-atom structures this distinction is no longer possible; both phenomena are involved, and it is important that the anomalous absorption coefficients for the atoms concerned be known to high accuracy.

For this paper we need to write the X-ray equations in the same form as the electron-diffraction equations, and for this purpose a nomenclature for X-rays in the electron-equivalent form. We start by defining the interaction constant σ, which by multiplication with the appropriate structure factor, results in a scattering probability per unit length. Thus $i\sigma_e V_h$ gives the kinematic (complex) scattering power per unit length for electrons , and $(\psi_h)_{kin} = i\sigma_e V_h \Delta Z$, gives the complex scattering amplitude in the first Born approximation, which requires that $\sigma_e = 2\pi/E\lambda(1+\beta^2)^{\frac{1}{2}}$ (Cowley, 1981), with the appropriate relativistic term deriving from the Klein-Gordon equations. Here V_h is the electron scattering factor in volts and ΔZ is the thickness of a crystal slice. An expression for the complete Born series in the high-voltage limit ($\lambda \rightarrow 0$) is then given as $\psi_h = \exp(i\sigma_e V_h \Delta Z)$, "thin phase grating" approximation (Cowley and Moodie, 1957), which approaches the exact solution in the limit $\Delta Z \rightarrow 0$. In a similar way $i\sigma_x F_h$ gives the kinematic (complex) scattering power per unit length for X-rays, requiring that $\sigma_x = r_c\lambda/\Omega$,where r_c = the classical electron (Davis, 1996).

Then, $\psi_h = \exp(i\sigma_x F_h \Delta Z)$, for N-beam dynamic X-ray diffraction in the equivalent high-energy limit, although the required approach to the limit $\Delta Z \rightarrow 0$ is reached for much greater ΔZ values than for electron diffraction, since $\sigma_e >> \sigma_x$, allowing the multi-slice to be used for far greater atomic weights that is the case for electron diffraction. Different approximations are required for electron and X-ray diffraction which relate to the much larger values of excitation error which give significant scattering in the electron case, directly related to the very much higher values of refractive index encountered in HEED. The expression for excitation error, $\zeta_h = \Delta k = k_0 - k_h$ in the linearised form, and for low-angle scattering, is still applicable in both cases, since $\Delta k << k_0$. However , the extinction distance, which can only be unambiguously in terms of the 2-beam approximation (or for N-beam cases which

reduce by symmetry to a 2-beam-like case), is given by the condition $\sigma_e V_h T = \pi$, for intensity extinction, where T is the total crystal thickness has a similar form $\ell_h = \pi/\sigma_e V_h$ and $\ell_h = \pi/\sigma_x F_h$, in both cases. The values however are very different due reasons given above, ($\sigma_e >> \sigma_x$). Furthermore the excitation error derived from the Ewald Sphere construction in approximation as $\zeta_h = \Delta k \cong 1/d_h \Delta\theta_B$, for θ_B small, is useful for high-voltage electron diffraction, but not for X-rays since the Bragg angles θ_B are now of the order of several degrees while $\Delta\theta_B$ is extremely small, and we need to use the exact expression, $\zeta_h = \Delta k = \tan(\Delta\theta_B)/d_h$, i.e. $[(\Delta\theta_B)/\theta_B]_{x\text{-rays}} >> [(\Delta\theta_B)/\theta_B]_{electrons}$. This is summarised in Table 1.

Treating Maxwell's equations as a vector form of the Schrödinger equation makes for a simpler physical understanding as well as simpler evaluation. The standard form of Maxwell's equations is due to Lorentz, and developed much earlier. The Schrödinger formulation leads naturally to Dirac-type factorisation as two coupled linear differential equations, which in turn allows the great simplification of using the S-matrix as an operator, by-passing the need to formulate Bloch-wave states in the crystal space, which are never required when considering elastic scattering (Heisenberg, 1944; Sturkey, 1962; Moodie, 1972). In dynamic X-ray scattering this comes about by Dirac-style linearisation of the second-order differential equation. The great value of this however lies in the ability to interpret these equations: Dirac's genius allowed him to relate these equations to electron and positron scattering respectively; in a parallel way Moodie realised that for X-rays the equations represented right- and left- handed circularly polarised states, σ^+ and σ^- (Wagenfeld and Moodie, 1972), a fact also recognised by Hillion (1979) under much more restricted conditions (see §1). The use of multi-slice (Goodman and Moodie, 1974) then becomes the procedure of choice for numerical evaluation.

NOTE: We found it difficult to avoid using the Greek symbol σ for both the interaction symbols and for the sign of the polarised X-ray beam, as σ^+ and σ^-, but believe that the interaction symbols expressed as σ_e and σ_x are sufficiently clearly

distinguishable to not introduce any confusion as to the meaning intended in the text content.

3. Results for CBXRAD patterns

We now show the results obtained for 3-beam orientations close to the 001 zone-axis orientation, for SiO_2 and $Os_5(CO)_{16}$, simulating for a wedge crystal to large as large thicknesses as permitted with realistic absorption factors (Chantler, 1994).

Both these belonging to the enantiomorphic space-group pair $P3_121$ and $P3_221$, for right-handed and left-handed structures respectively (Lang, 1965). In both cases the unit cell contains 3 molecules; metal ion those space-groups occupying the 3(a) site in SiO_2 (Wykoff, 1948) and (3a) and 6(c) sites in $Os_5(CO)_{16}$ (Reichart and Sheldrick, 1977). The calculations were made for 3-slices per unit cell, using single-molecule projections. To slice through these thicknesses within a reasonable time a cray-computer was used. $MoK\alpha_1$ and $TaK\alpha_1$ wavelengths were chosen for SiO_2 and $Os_5(CO)_{16}$ respectively, to minimise anomalous absorption. We chose thicknesses sufficiently great so that the intensity filled as much of the aperture field, with an aperture subtending approximately 90 mrad at the crystal for SiO_2 , while for $Os_5(CO)_{16}$ this angle is 140 mrad. This corresponds to an excitation error range of ζ_h ± 0.07 for SiO_2 , and of ± 0.01 for $Os_5(CO)_{16}$, where $\zeta_h = \lambda/2\cos\theta_B = \tan(\Delta\theta)/d_h$.

These conditions have led to intensities, expressed as fractions if the normalised incident beam as unity, in the $10^{-11} \rightarrow 10^{-12}$ for SiO_2 , and $10^{-9} \rightarrow 10^{-12}$ for $Os_5(CO)_{16}$ in the diffracted beam.

Visual analysis of the 100 and 010 diffraction disks produced for SiO_2 under conditions of a equilateral triangle in diffraction space, show a subtle change in the outer pattern, for these reflections, especially when analysed for left-hand-transmitted intensities with a right-handed incident state, and when changing from right-handed to left-handed input radiation (see Fig. 1). The symmetry relationship between the pair is *not so obvious, until the more observable results from the same reflection pairs (100* and 010) and space groups for $Os_5(CO)_{16}$ (Fig 2) are seen. However this is most probably related as much as anything else to exposure time. For the weaker scatterer

(SiO_2), had a sufficiently longer exposure been used, this would simply have over-exposed the central-pattern details to a constant white, but allowed the more significant higher excitation error regions to be examined in more detail.

Before attempting to interpret the apparent symmetries appearing we should first analyse the expected results, using reciprocity. Fig. 3 shows how reciprocity, which we now understand in terms of time-reversal symmetry (Goodman and Gunning, 1992), behaves for circular-polarise X-rays passing through a chiral structure. The central part for the left and right boxes are related by a mirror reflection, which acts to change the crystal hand. In each case the reciprocal paths are indicated by dashed lines. It is to be noted that these are <u>not</u> mirror-reflected (see Moodie, 1972), since the time arrow is irreversible. However the hand of the radiation (both in and out) does change hand. Analysis of this figure allows one to see two key points. The first is that for a single crystal of either hand, now exact mirror symmetries can be expected. This is another way of saying that for X-ray transmission through thick crystals the projection approximation (Buxton, Eades, Steeds and Rackham, 1976) <u>never</u> holds. The second point of some interest is that if we compared the diffraction from the two structures, $P3_121$ and $P3_221$ separately, the reciprocal beams from the one should mirror the direct beams from the other. This mirror relationship occurs due to the reversal of sign in ζ_h , brought about by the reciprocity relationship in diffraction (Pogany and Turner, 1968).

Returning now to Figs. 1 and 2, this mirror relationship is seen between the two computed disks on the right side of the diagrams; the lack of exact mirror symmetry between beams *g* and *h* (100 and 010) which have the same $|F_h|$ values and the same excitation-error conditions (under symmetrical illumination) is also detectable, in intensity and also in fine details of outer fringes. This agreement with theoretical prediction also justifies the parabolic approximation used for these multi-slice simulations; *the same approximation is also used in HEED, but not an essential* condition for multi-slice formulation which can also be programmed for a true sphere.

There is no equivalent situation for electron diffraction unless we consider magnetic domains, when a reversal of the magnetic vector is required to produce a reciprocity relationship. This is not considered in standard CBED symmetry theory (Buxton, Eades, Steeds and Rackham, 1976).

Its observation confirms our ideas that cyclic rotation of phases occurs within the 3-beam pattern, which is mirror-symmetric only in projection.

The precision with which we can observe this mirrored symmetry justifies the approximations which have been made in the multi-slice calculations for relatively low-angle forward scattering, namely that of a parabolic propagation envelope instead of the actual Ewald sphere section involved. Although this approximation is not basic to multi-slice, it is a convenient simplifying component of standard multi-slice procedure in electron diffraction.

More significantly, the operation of diffraction phases in causing these asymmetries confirms our belief that cyclic terms in the 3-beam diagram which end up on diffraction order (i.e. for $N=2+3n$, were n, is an integer, $0< n<\infty$,), play a significant role in determining hand by chiral interaction (see also Moodie, Etheridge and Humphreys, 1996).

3. Alternative Presentation of Results in Pendellösung Form

Alternative forms of presentation of the computed results allow a more quantitative assessments of points already discussed and displayed in the DBXRAD figures of the previous section.

The first method we will use is that of a rocking curve, which may be obtained by using an accurate goniometer.

At first we have displayed the rocking curves obtained for the two compounds. This shows at least for computational analysis, a more quantitative idea of some of the phenomena observed in the DBXRAD patterns of Figs. 1 and 2. Fig, 4 shows in the upper curve the results for SiO_2 ,using MoK_{α_1} radiation, while the lower curve shows at a similar intensity level, the results for $Os_5(CO)_{16}$, with more widely spread subsidiary maxima. Across the curves at specific levels, horizontal lines have been

drawn to allow a judgement to be made about the pattern asymmetry, for the two cases of (a) simulations for a projected structure (one slice per unit cell) and (b) simulations for the non-projected structure in which we take 3 slices per unit cell. We now see that even with the so-called projected structure, where chirality can play no part, a failure of the "projection approximation", as it is called for HEED, and which would require a symmetry of the space group P3/m (Moodie and Whitfield, 1996). This failure has already been remarked on in the previous section.

Then, the left side of the diagram showing simulations for the non-projected chiral structure shows a much greater asymmetry across the rocking curves, increasing as the order of subsidiary maxima increases. This has also been noted above, but from these curves we see that it is just as visible for the light-atom structure (SiO_2) as for $Os_5(CO)_{16}$, showing that it is by no means impossible to use this much more readily available compound for an experiment, which requires in addition a much more accessible radiation as far as a synchrotron source, and capillary optics, is concerned.

An alternative presentation of the results in Pendellösung form, such has been obtained in the past by use of the Lang Camera (see §**1**), which provides much more detail in quantitative form for a variety of conditions. For the following wedge-crystal Pendellösung figures we have chosen different orientations, namely an equilateral triangle in diffraction space including the central beam and the $02\bar{2}0, 2\bar{2}00$, reflection pair, simply because these reflections have larger F_h, F_g, values than the $01\bar{1}0$, $10\bar{1}0$, reflections. Also from here on we shall use the *hkil* notation for the trigonal (hexagonal) systems, to avoid any confusion which could arise from the shortened notation *hkl*, especially when we compare the 3-beam and 6-beam calculations, with defined zone-axis coordinates [*uvwl*].

Fig. 5 then shows the results for the 3-beam case, 0000, $2\bar{2}00$, and $02\bar{2}0$ reflections, as a function of thickness, for SiO_2 ,using MoK_{α_1} radiation. These curves are for the summed intensities of the same reflections, i.e. *g* and *h* reflections concerned (without the central beam), to show the difference between computations made using one-slice per unit cell, (the two central curves, with those made for 3-slices

per unit cell, (the upper and lower sets of curves) for ζ_h values of ± 0.3. What this figure shows then is that for a crystal of fixed hand (here for right-handed quartz), there is a very much greater asymmetry in the dynamic shape function than for the non-chiral structure (which still shows some response to change of excitation-error sign). This is shown we believe more quantitatively than the DBXRAD patterns of the previous section.

Fig.6 then shows, for the same radiation (right-handed incidence) the 3-beam case for the beams $02\bar{2}0, 2\bar{2}00$, and 0000, the difference between the transmitted beams of left-handed polarisation, through left-handed quartz and right-handed quartz respectively, made by the one-slice (lower curve) and 3-slice method, over a similar thickness regime. Here again we see the quantitative significance of the chirality interaction. This interaction appears to be strongest when the output beam is monitored for the polarisation state opposite to the incident polarisation state (see also the conditions for the DBXRAD simulations).

Figs. 7 and 8 now refer to the $Os_5(CO)_{16}$ structure using TaK_{α_1} radiation. Fig.7 then shows the effect of changing the sign of excitation error for ζ_h values of ± 0.1. For the heavier atom structure we now see the much greater difference between the simulations for excitation error has on separating the chiral structures, i.e. in the ability to determine crystal hand, and using a 3-times smaller deviation from θ_B . Admittedly the thickness regime is greater, but nevertheless the intensity values on an absolute scale are not too different.

Finally, Fig. 8 shows the effect of including 6 beams in the dynamic simulations. In this case we show the difference between the 3-beam case (upper curve) and the 6-beam case (lower curve) for the closest beam, $2\bar{2}00$. The diffraction conditions for the 6-beam case are as follows: the central beam is aligned near the [0110] direction, giving six Bragg points in a hexagon, namely , $2\bar{2}00$, $\bar{2}4\bar{2}0$. $08\bar{8}0$, $22\bar{4}0$, $20\bar{2}0$ and 0000, examining the same output beam in both cases. There is obviously not much advantage to be gained in the 6-beam interaction for this close-in reflection $2\bar{2}00$. However indications from trial calculations for the most distant

reflection, namely the $44\bar{8}0$ reflection, that much better sensitivity can be gained by using small values for $|\zeta_h|$, but at the cost of much reduced intensities.

4. Suggested Experimental Procedures.

Because of the very weak beams we are examining in the CBXRAD technique, and the requirement for polarised X-rays, synchrotron radiation was a natural choice for any experimental observation of the symmetry relationships we have predicted by the above computations. Then, the technique described by Baliac *et al.*, (1996) shows that at least for soft X-rays (up to say the MoK_{α_1} wavelength), it is possible to produce a focus some mms from the exit of the capillary. This would allow space for the sample, controlled by a goniometer, and has been demonstrated by the above authors, this has produced disk-shaped diffraction orders at some distance from the sample the focal point (or back-focal plane). In order to simulate the conditions of LACBED we would also need to insert a circular aperture in the back-focal-plane in of such dimensions as to eliminate all diffuse scattering in neighbouring reciprocal space, an tightly define the particular diffraction order of interest. This has been effective in LACBED in eliminating almost all diffuse scattering, that is to say, all inelastic scattering such as that forming the Kossel (or Kikuchi) lines and bands, especially that due to TDS which tends to be high-angle scattering. This would also be an essential component of any CBXRAD experiment, since we are calculating here only for elastically scattered X-rays, although with anomalous absorption included.

However there are two serious problems with the type of focus achieved by the above authors. One is that the focus is highly concentrated around the directly-transmitted ray, and falls of rapidly across the disc from the centre outwards. The second problem is that the type of glass used by them would not suit such hard radiation as TaK_{α_1}.

On the other hand, Bilderback, Thiel, Pahl and Brister (1994) have suggested the use of lead-glass for hard radiation, which carries with it an increased fluorescence from the capillary together with a less efficient central focussing. This fluorescence

may in fact be a factor which would spread the radiation more evenly across the outgoing disc. Clearly more experimental work needs to be done on testing different capillary designs, including the use of a "diffuser", to determine conditions most suitable for CBXRAD work.

It is also possible that for hard radiations such as TaK_{α_1}, a laboratory rotating-anode source may be more suitable, in which case the beam would need to first pass through a linear-polarising element, such as used by Hart and Lang (1965), and then through a 1/4 wave plate to achieve a circularly-polarised beam. Certainly their arrangement using a Lang Camera would be most suitable for obtaining the wedge-crystal results shown in Figs.4 - 7 of this paper.

These matters are currently under investigation.

5. Discussion.

There are many points of interest which have arisen from the present results. First we have the significant but small departure from the projection approximation for thick-crystal X-ray diffraction, and the revised form of reciprocity needed to handle enantiomorphic structures. These at least are of interest to the Electron Diffraction community.

At a more basic level, the is an interest in the symmetrical 3-beam problem in X-ray diffraction, long considered though not published (to our knowledge) by Prof. A.F. Moodie. There is indeed some comparison to be made between this triangular scattering loop, which transmits σ^+ radiation much more strongly into the crystal of similar hand ($P3_121$) than σ^-, (and equally σ^-, transmits more strongly through the $P3_221$ structure), and the operation of a 3-phase motor, which will only start in a particular direction. The difference here is essentially the difference between a 2- and 3-dimensional problem.

Another question bound to be asked is, is this discovery, of detection of chirality by X-rays purely abstract, considering that the same distinctions can much more readily made with visible light? We are strongly of the opinion that this testing, of phenomena known in the visible optics region, in the wavelength regime of X-rays

establishes important points in scattering theory, which we already feel assured, will lead to other and better formulations of the dynamic theory of X-rays. Some of these authors are started now, as a consequence of the present work, on a new formulation for dynamic X-ray scattering.

Since this work has been contemplated for some years we find that before the present work, in any group of theoretical physicists, the majority have said "this will never work", while a minority have said "the results will be positive but that is so obvious that is not worth investigating". In this debate we hold the middle ground.

We would like to conclude on a positive basis by paying tribute to the life-long and highly original personal theoretical thought put in by A.F. Moodie over a period of 40 years, which continues in 1998, and which we who were lucky enough to have him as supervisor for a period have learnt so much basic scattering physics. Typically of this scientist, most of his work was black-boarded as private discussion, and never published. We can only wish him a continuing and outstanding future.

5. Acknowledgments.

We wish to acknowledge invaluable assistance from the following members of our School: Chris Chantler, Peter Paterson, Simon Matheson, and David Kube.

Last but not least, one of us (P. Goodman) wishes to acknowledge continuous encouragement throughout this project given by Geoff Opat and Tony Klein, the leaders of the "Fundamental Experiments Group" within our School.

This research was partly funded by a Visiting Young Asian Scholarship awarded by Melbourne University.

References

Baliac, D.X. Barnea, Z., Nugent, K.A, Garret, R.F. Varghese, J.N. aand Wilikens, S.W.(1996). J. Synchrotron Rad. 1. 37-42.

Bilderback, D.H., Thiel, D.J. Pahl, R. and Brister, K.E. (1994). J. Synchrotron Rad. 1. 37-42.

Buxton, B.F., Eades, J.A., Steeds, J.W. and Rackham, G.M. (1976). Philos. Trans. R. Soc. London Ser. A, 281, 171-194.

Chantler, C.T. (1994). Resonant Anomalous Scattering-Theory and Applications. edited by G, Materlik and K. Fischer. Elsevier Science B.V.

Cowley, J.M. (1981). Diffraction Physics:2nd Edition. p.4, North-Holland Publ. Co.

Davis, T. J. (1994). Acta Cryst., A50, 686-690.

Engström, P., Larssen, S., Rindby, A., Buttkewitz, A., Garbe, S., Gaul, G., Knöchel, A. and Lechtenberg, F. (1991). Nucl. Instrum. Methods, A302, 547-552.

Goodman, P. and Gunning, J. (1992). Acta Cryst. A48, 591-595.

Hart, M. and Lang, A.R. (1965).Acta. Cryst.,19, 73-77.

Hart, M. and Milne, A.D. (1968). Phys. Stat. Sol. 26, 185-189.

Hart, M. and Lang, A.R. (1965). Acta Cryst. 19, 73-77.

Heisenberg, W. (1944): cited in: Pions to Quarks (1989). edited by L. M. Brown, M. Dresden, and L Hoddeson: The Early S-Matrix Theory and its Propagation, 1942-1952. Cambridge University Press.

Hillion, P. (1979). J. Optics (Paris), 10, 21-30.

James, R.W. (1963). Solid State Physics. Vol.15. edited by F. Seitz & D. Turnbull.Academic Press.

Lang, A. R. (1962). Proceedings of the International Conference on Crystal Lattice Defects. J. Phys. Soc. Japan, 18, Suppl. 2, 332.

Moodie, A.F. (1972). Dynamical N-beam theory of electron diffraction. Encyclopedea dictionary of physics. Subppl. 4. edited by A. Thewlis.

Moodie, A.F. (1972).Zeits. für Naturforsh. 27a, 437-440.

Moodie, A.F., Etherige, J. and Humphreys, C.J. (1996). Acta Cryst. A52, 596-605.

Moodie, A.F. and Wagenfeld, H. (1975). Acta Cryst. A31, S249.

Moodie, A.F. and Whitfield, H. J. (1994). Acta Cryst. A50, 730-736.

Pogany, A.P. and and Turner, P.S. (1968). Acta Cryst. A24, 339

Reickart, E. and Sheldrick, G.M.(1977).Acta Cryst., B33, 173-175.

Sakurai, J. J. (1967). Advanced Quantum Mechanics. Addison-Wesley Publishing Co. p169 (footnote).

Sturkey, L. (1962) Proc. Phys. Soc. 80, 321.

Theil, D.J., Stern, E.A., Bilderback D.H., and Lewis, A. (1989). Physica B158, 314-316.

Weckert, E. and Hümmer K. (1997). **A53**, 108-143.

Wykoff, R. W. G. (1948). *Crystal Structures*, Vol. 1. New York: Interscience.

ELECTRONS	V_h (volts)	$\sigma_e=2\pi/E\lambda(1+\frac{1}{2}(1-\beta^2)^{\frac{1}{2}})$	$\ell_h = \pi/\sigma_e V_h$
X-RAYS	F_h (electrons)	$\sigma_x = r_c\lambda/\Omega$	$\ell_h = \pi/\sigma_x F_h$

TABLE 1.

Comparison between Scattering Terms for Dynamic Electron diffraction and Dynamic X-ray diffraction.

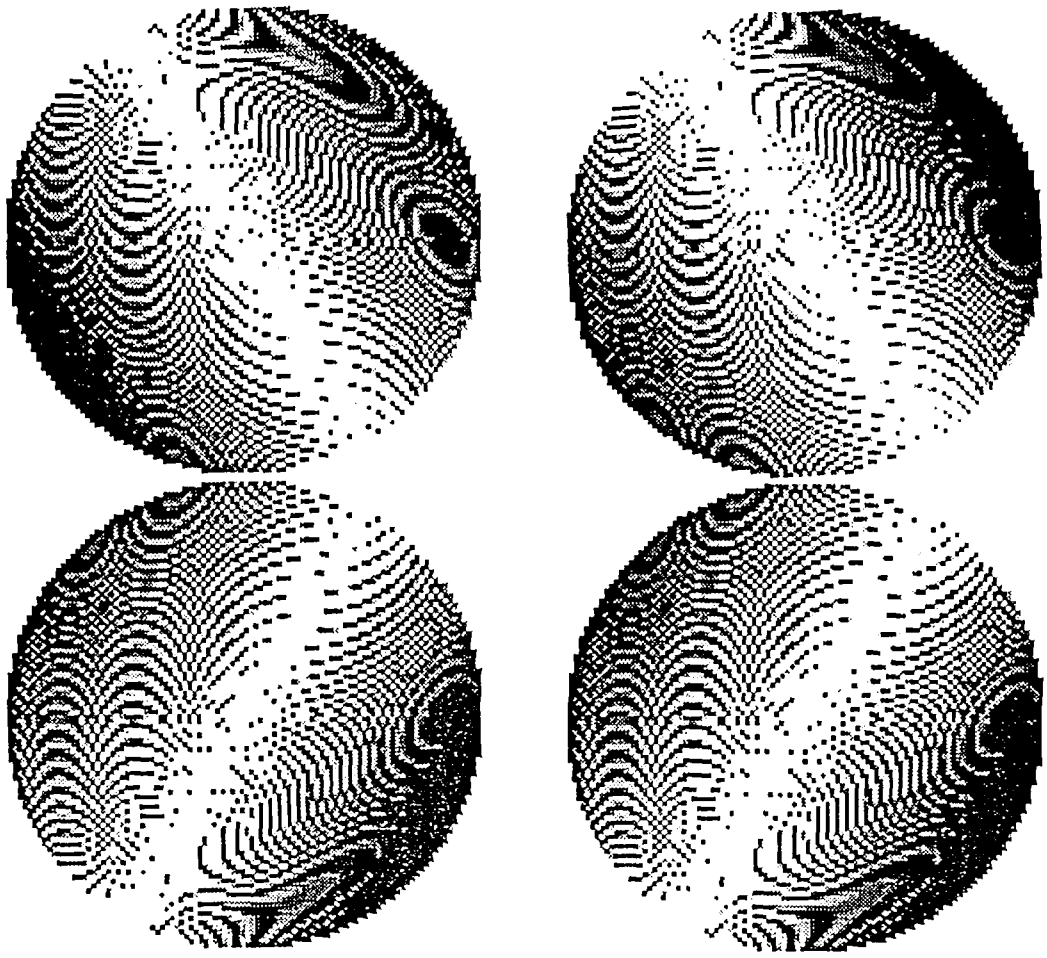

Fig.1

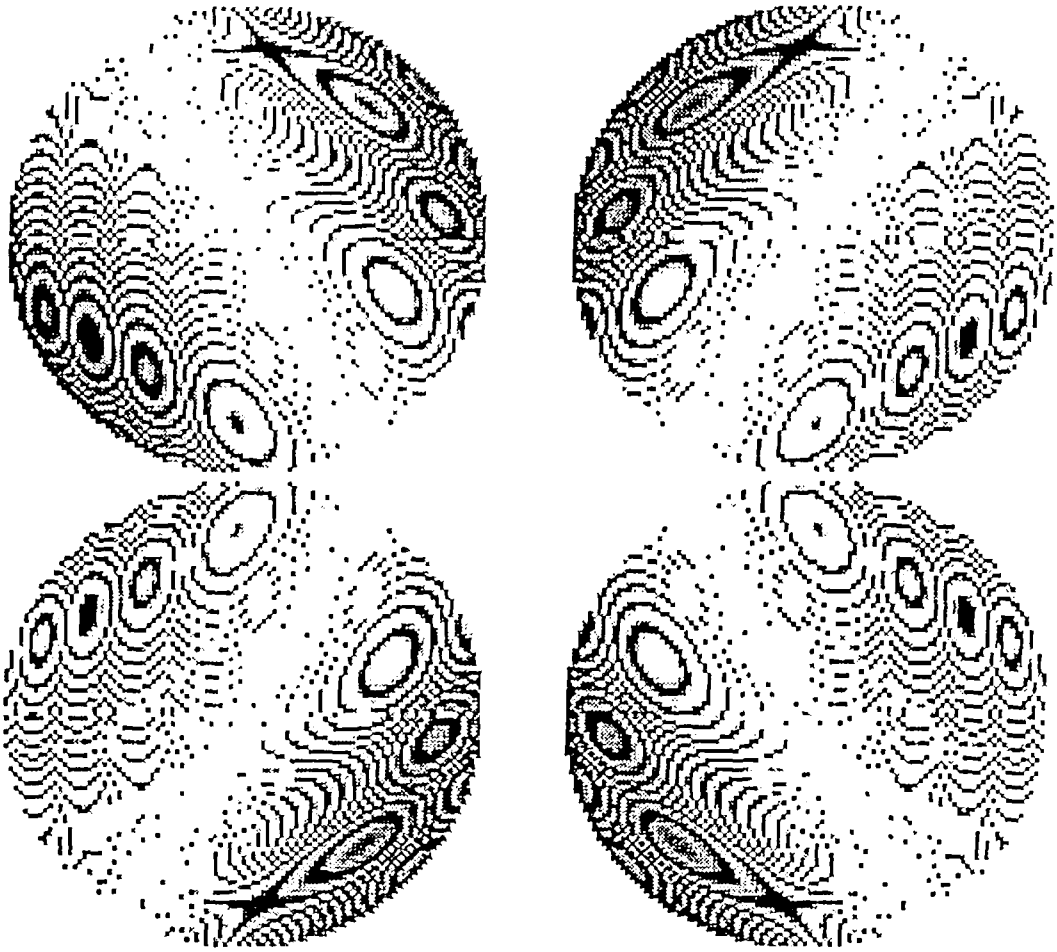

Fig.2

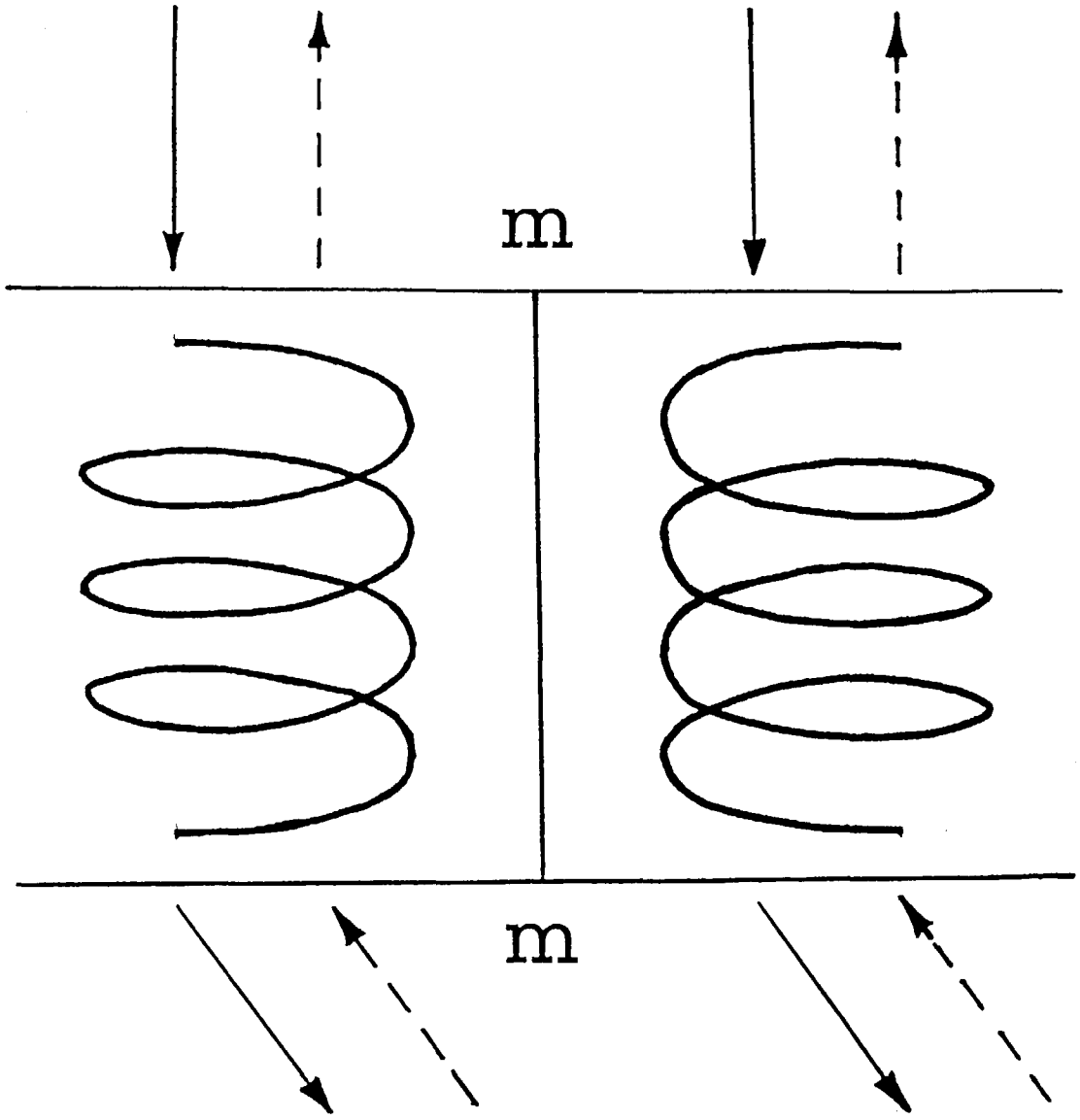

Fig.3

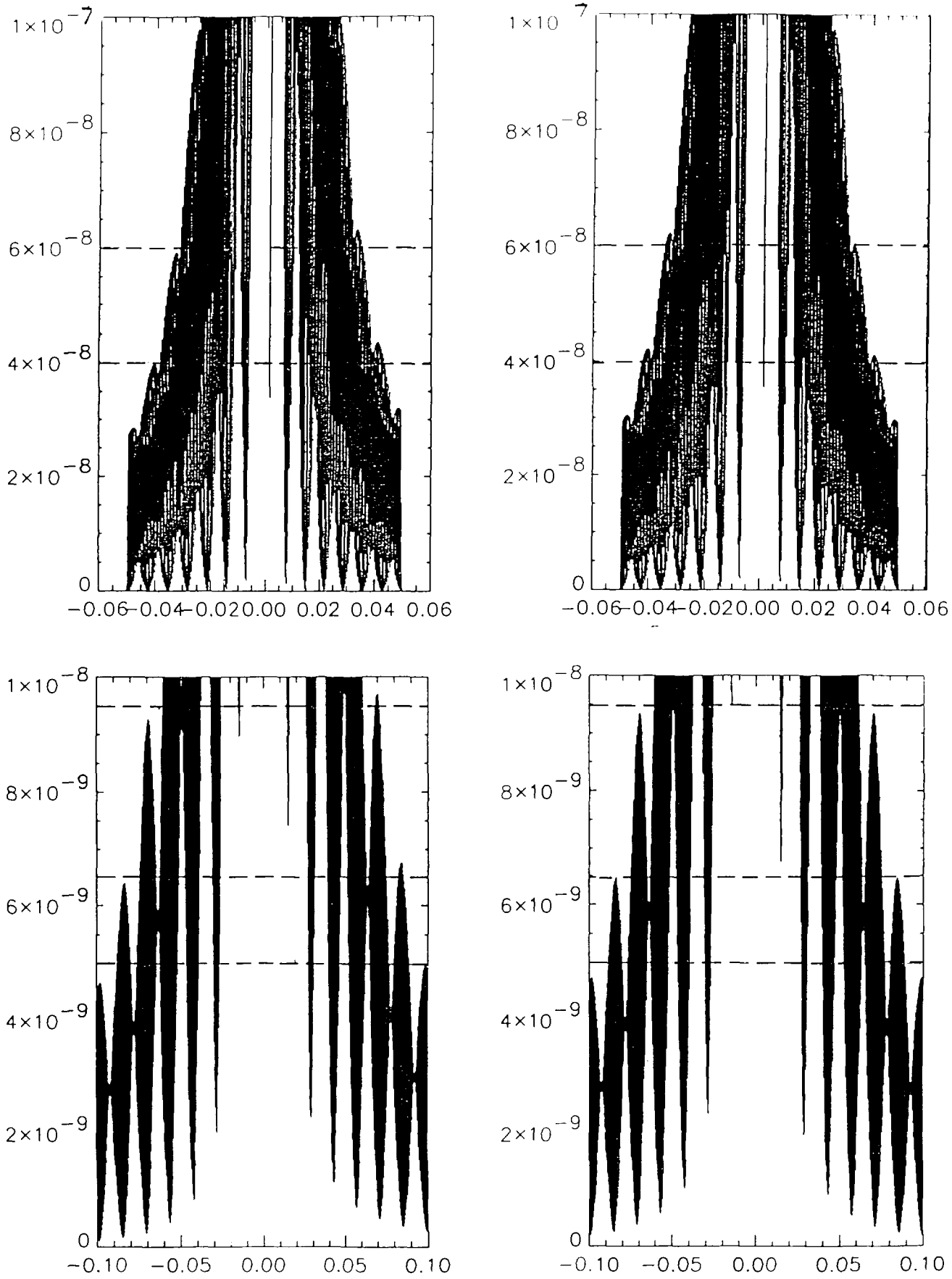
1×10⁻⁷
8×10⁻⁸
6×10⁻⁸
4×10⁻⁸
2×10⁻⁸
0
−0.06 −0.04 −0.02 0.00 0.02 0.04 0.06
1×10⁻⁷
8×10⁻⁸
6×10⁻⁸
4×10⁻⁸
2×10⁻⁸
0
−0.06 −0.04 −0.02 0.00 0.02 0.04 0.06
1×10⁻⁸
8×10⁻⁹
6×10⁻⁹
4×10⁻⁹
2×10⁻⁹
0
−0.10 −0.05 0.00 0.05 0.10
1×10⁻⁸
8×10⁻⁹
6×10⁻⁹
4×10⁻⁹
2×10⁻⁹
0
−0.10 −0.05 0.00 0.05 0.10

Fig.4

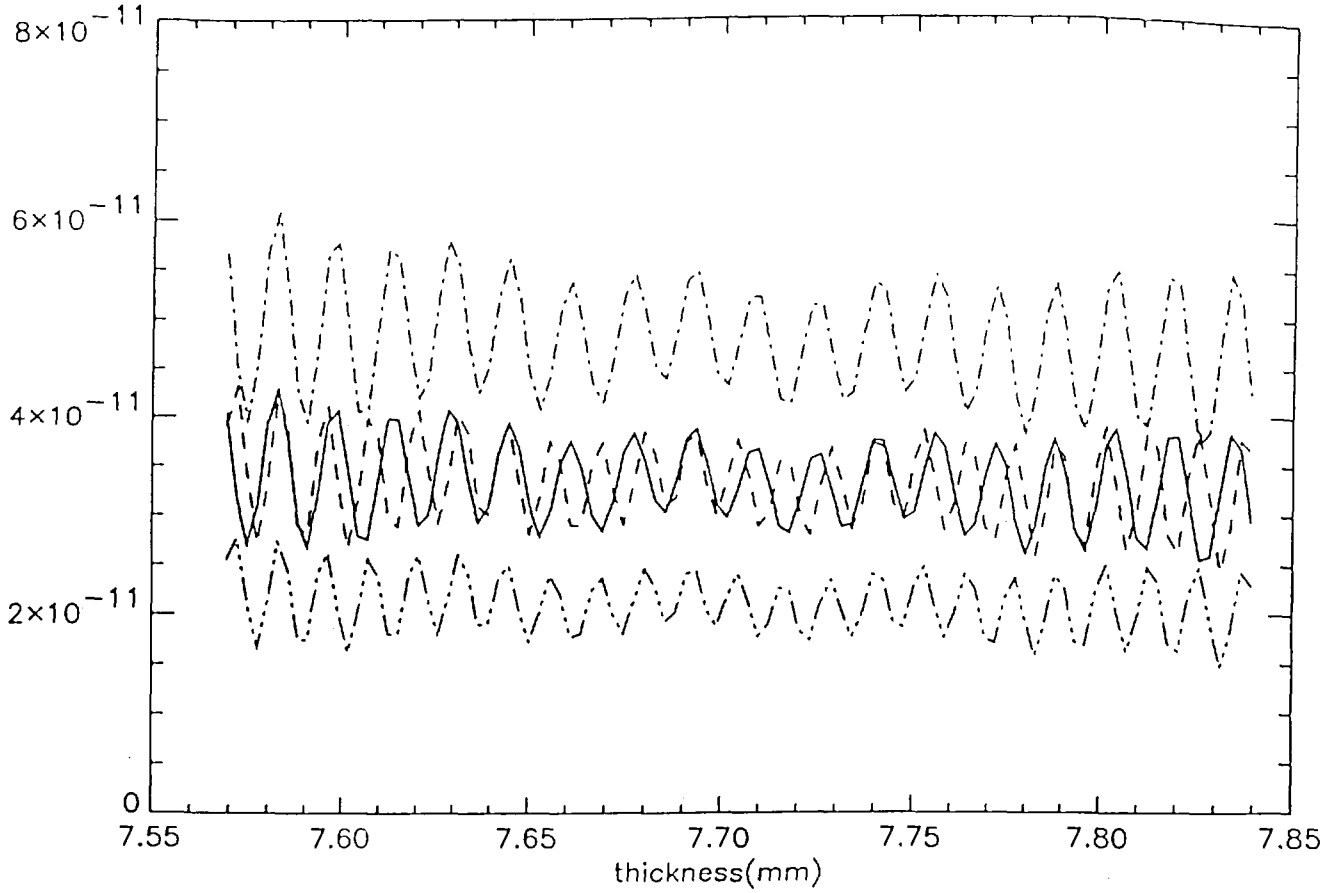
8×10⁻¹¹
6×10⁻¹¹
4×10⁻¹¹
2×10⁻¹¹
0
7.55
7.60
7.65
7.70
7.75
7.80
7.85
thickness(mm)

Fig.5

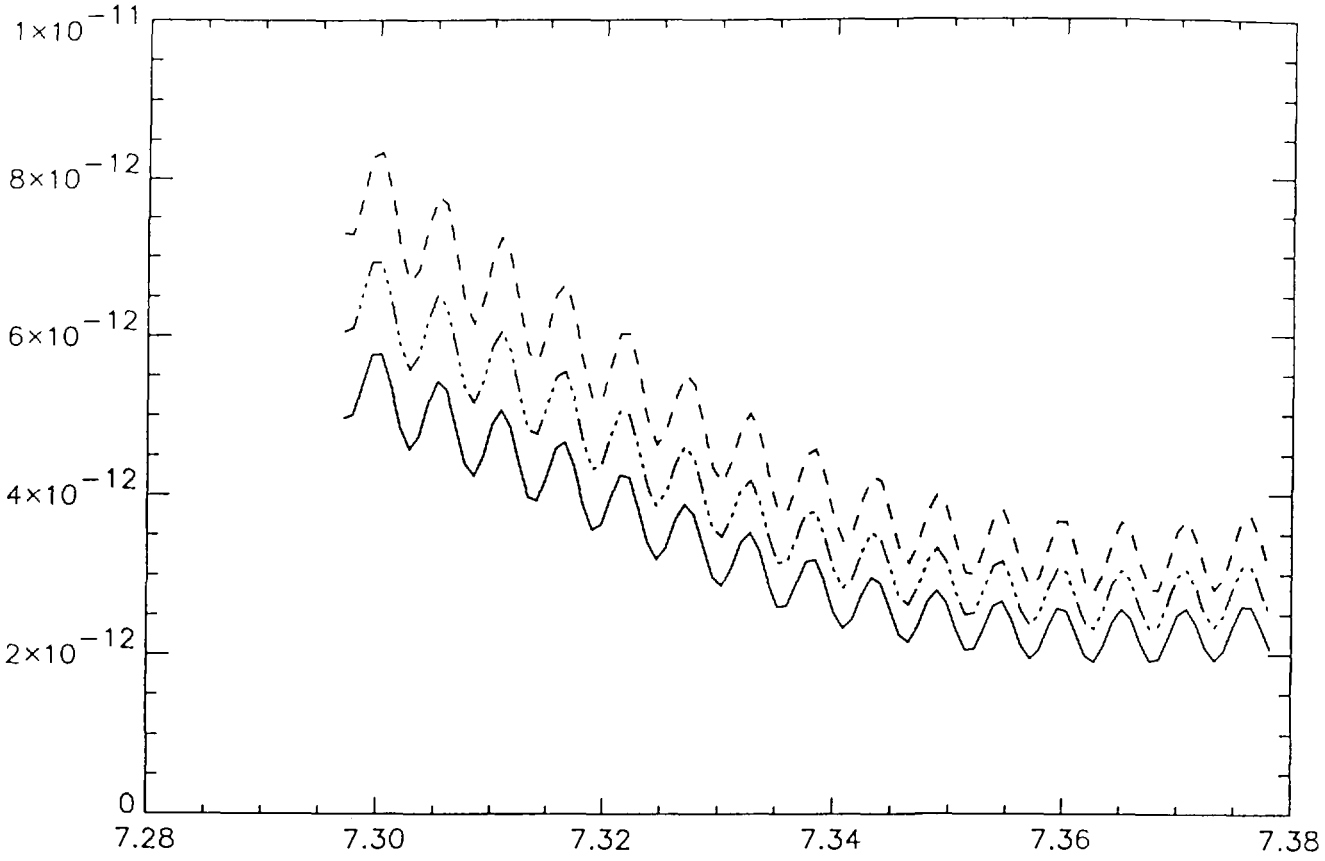

Fig.6

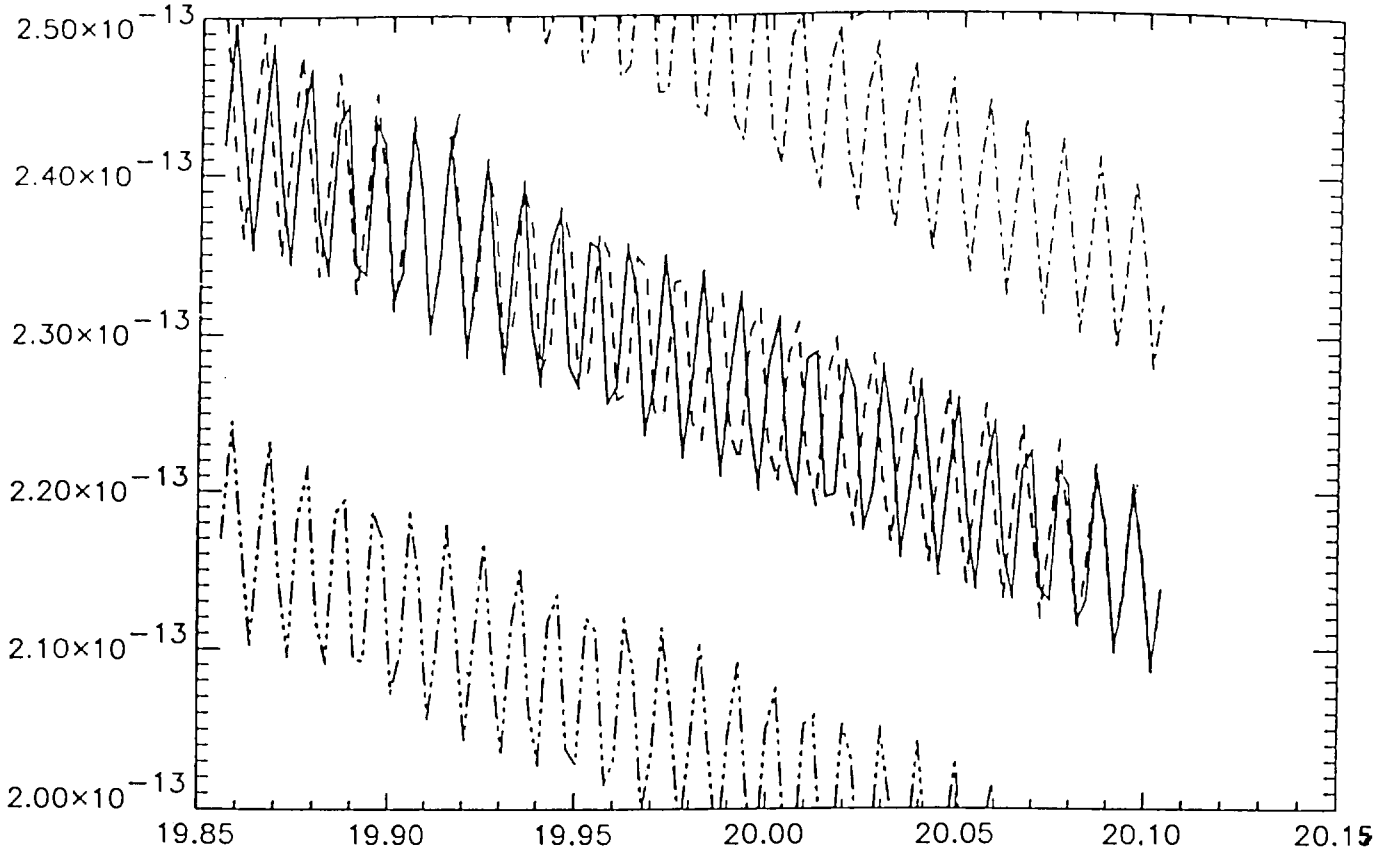
2.50×10⁻¹³
2.40×10⁻¹³
2.30×10⁻¹³
2.20×10⁻¹³
2.10×10⁻¹³
2.00×10⁻¹³
19.85
19.90
19.95
20.00
20.05
20.10
20.15

Fig.7

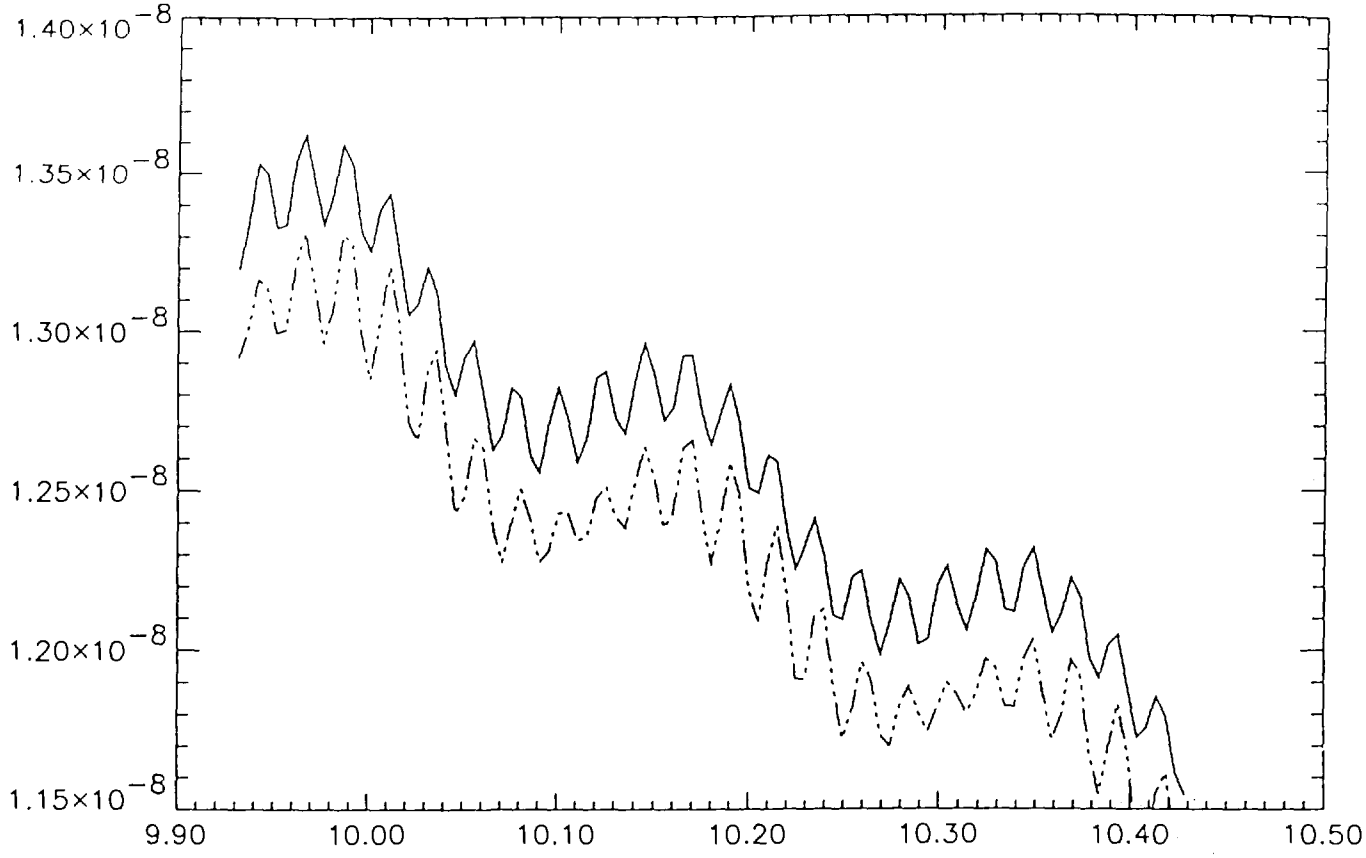
1.40×10⁻⁸
1.35×10⁻⁸
1.30×10⁻⁸
1.25×10⁻⁸
1.20×10⁻⁸
1.15×10⁻⁸
9.90
10.00
10.10
10.20
10.30
10.40
10.50

Fig.8

FIGURE CAPTIONS.

Fig.1. This set of four figures is numbered (a) - (d) in clockwise rotation from the upper left. Figs. I(a) to (d) then show the DBXRAD patterns for the 100 and 010 reflections respectively for the symmetrical 3-beam case, with an equilateral triangle 000, 100, 010, for α-quartz and MoK_{α_1} radiation, and for the conditions of a right-handed circularly-polarised state, σ^+, incident and the opposite state , σ^- selected for the output beam. Figs I(a) and (c) are for the right-handed form ($P3_121$), and Figs. 1(b) and 1(d) are for the left-handed form ($P3_221$).

Fig.2. These figures (a) to (d), numbered in the same way as for Fig.1, show results for the $Os_5(CO)_{16}$ structure, for the same 3-beam case (000, 100, 010), using TaK_{α_1} radiation, with the same meanings for (a) to (d) as in Fig.1.

Fig.3. Diagram showing the reciprocity relationship, together with a mirror reflection which acts only on the crystal, and radiation chiralities, and not on the reciprically-related beams. These latter are indicated by dashed-line arrows, while the direct beams are indicated by full-line arrows.

Fig.4. Rocking curves obtained for α-quartz (upper curves), and for $Os_5(CO)_{16}$, by the same 3-beam interaction as used for Figs. 1 and 2. Horizontal dashed lines at specific levels are a guide to the degree of asymmetry in the curves in the subsidiary maxima, about the central peak.
On the right side the curves are simulated by the 1-slice method (unit-cell projection), while those on the left side are simulated for the 3-slice method (allowing chiral interaction along the z-axis to be displayed.

Fig.5. Results for the 3-beam case involving the reflection set $02\bar{2}0$, $2\bar{2}00$, and 0000, in symmetrical triangle excitation, for α-quartz and MoK_{α_1} radiation, for the summed $02\bar{2}0$ and $2\bar{2}00$ intensities, again for σ^+ incidence and σ^- analysed output. The central curves are for the 1-slice simulation, and the upper and lower curves are for the 3-slice simulations, for ζ_{lh} values of ± 0.3

(upper and lower curves respectively), and for the central curves these values are represented by full and broken lines respectively.

Fig.6. These curves are for the α-quartz structure, for 3-beam case ($02\bar{2}0, 2\bar{2}00$, and 0000), using TaK_{α_1} radiation. These curves show the effect of change of sign of excitation error, for ζ_h values of ±0.3. All curves are the summed diffraction intensities; the upper curve (broken line) is for the right-handed structure using the 3-slice computational method, the second curve (intermittent broken line) is for the left-handed structure simluated by the same method, while the lowest curve (full line) is for the 1-slice simlation method (i.e. for a projected unit cell).

Fig.7. This figure shows the diffence between then 3-beam case and the 6-beam case, following the effect changing the sign of excitation error for ζ_h values of ±00.1, for the same 3-beam case following the $02\bar{2}0, 2\bar{2}00$, and 0000, set and the $2\bar{2}00$, $\bar{2}4\bar{2}0$. $08\bar{8}0$, $22\bar{4}0$, $20\bar{2}0$ and 0000, set respectively, using TaK_{α_1} radiation. The 3 curves have the same meaning as those for Fig. 6.

Fig.8. This figure shows simulations for both the 3-beam and 6-beam cases, the latter including the reflection set $2\bar{2}00$, $\bar{2}4\bar{2}0$. $08\bar{8}0$, $22\bar{4}0$, $20\bar{2}0$ and 0000. The 3-beam case (upper curve) and the 6-beam case (lower curve) are both for the $2\bar{2}00$ beam intensity.